Effects of magnetic field strength and particle aggregation on relaxivity of ultra-small dual contrast iron oxide nanoparticles

Materials Research Express

PAPER

Effects of magnetic field strength and particle aggregation on relaxivity of ultra-small dual contrast iron oxide nanoparticles

RECEIVED
20 July 2017

REVISED
25 October 2017

ACCEPTED FOR PUBLICATION
30 October 2017

PUBLISHED
13 November 2017

Hang T Ta[1,2], Zhen Li[3], Yuao Wu[1], Gary Cowin[4], Shaohua Zhang[3], Anya Yago[5], Andrew K Whittaker[1,2,4] and Zhi Ping Xu[1]

[1] Australian Institute for Bioengineering and Nanotechnology, The University of Queensland, Brisbane, Australia
[2] ARC Centre of Excellence in Convergent Bio-Nano Science and Technology, Brisbane, Australia
[3] Center for Molecular Imaging and Nuclear Medicine, School for Radiological and Interdisciplinary Sciences (RAD-X), Soochow University, Collaborative Innovation Center of Radiation Medicine of Jiangsu Higher Education Institutions, Suzhou 215123, People's Republic of China
[4] Centre for Advanced Imaging, The University of Queensland, Brisbane, Australia
[5] Centre of Microscopy and Microanalysis, The University of Queensland, Brisbane, Australia

E-mail: h.ta@uq.edu.au

Keywords: dual contrast iron oxide nanoparticle, magnetic resonance imaging, magnetic field strength dependence, aggregation, relaxivity

Abstract

This study aims to compare the relaxivities of ultra-small dual positive and negative contrast iron oxide nanoparticles (DCION) at different magnetic field strengths ranging from 4.7 to 16.4 T at physiological temperatures; and to investigate the effect of particle aggregation on relaxivities. Relaxivities of DCIONs were determined by magnetic resonance imaging scanners at 4.7, 7, 9.4, and 16.4 T. Both longitudinal (T_1) and transverse relaxation times (T_2) were measured by appropriate spin-echo sequences. It has been found that both longitudinal and transverse relaxivities are significantly dependent on the magnetic field strength. Particle aggregation also strongly affects the relaxivities. Awareness of the field strength and particle colloid stability is crucial for the comparison and evaluation of relaxivity values of these ultra-small iron oxide nanoparticles, and also for their medical applications as contrast agents.

Introduction

Magnetic resonance imaging (MRI) has become a powerful and indispensable tool in medical research, clinical diagnosis, and patient-care since 1977 [1, 2]. Unlike positron emission tomography (PET) or computed tomography (CT), MRI does not employ ionizing radiation; unlike ultrasound and optical methods, MRI provides deep tissue penetration; and it is more advantageous than PET, because MRI has much higher spatial resolution (sub-millimeter) [3]. Gadolinium (Gd) contrast agents are widely used and can give T_2/T_2^* (where T_2^* is observed or effective T_2) signal nulling for dynamic susceptibility contrast (DSC) and T_1 signal enhancement for dynamic contrast enhanced (DCE) imaging. Iron oxide nanoparticles, typical negative or T_2/T_2^*-weighted contrast agents, generally provide negative image contrast due to T_2/T_2^* shortening. DCE imaging allows easier detection of enhanced areas in the tissue compared to T_2/T_2^* nulling methods because of the potential confusion with image null areas due to air, cortical bone, tissue interfaces, hemorrhage or signal cancellations at water-fat interfaces [4]. On the other hand, T_2-weighted imaging via iron oxide nanoparticles is widely explored as iron is naturally found in the body [5]. In addition, susceptibility agents give image effects larger than the physical size of the region of agent localization.

Several diagnostic methods combine complementary information obtained from different imaging techniques (i.e. MRI, PET, CT and optical microscopy) to achieve higher accuracy of disease diagnosis [6–9]. However, the development of dual diagnostic strategies that employ a single imaging technique and a single instrumental system such as MRI is preferred because differences in depth penetrations and spatiotemporal resolutions of various imaging devices can lead to difficulties and discrepancies when matching images, resulting in interpretation inaccuracies [6, 7]. Therefore, in the last decade, ultra-small dual positive and negative contrast iron oxide nanoparticles (DCION) have been widely developed to overcome the disadvantages of single modality contrast agents in MRI [3, 5, 10–16], and the use of these dual contrast nanoparticles for molecular imaging

has been reported. For example, we synthesized and developed ultra-small, water-soluble and biocompatible magnetic iron oxide nanoparticles as positive and negative dual contrast agents for targeted imaging of thrombosis [3]. In another example, Xue *et al* [17] reported the use of 3.5 nm iron oxide nanoparticles for dual-modality MRI of tumor angiogenesis.

The reported dual MRI contrast iron oxide nanoparticles show good longitudinal and transverse relaxivities r_1 (4.4–19.7 mM^{-1} s^{-1}) and r_2 (17.5–60 mM^{-1} s^{-1}) with low r_2/r_1 ratios (1.4–3) at low magnetic field strengths (1.5–3.0 T) [11–16]. However, there have been limited reports on their relaxivities at higher magnetic field strengths. State-of-the art clinical MRI devices use magnets of high field strength, i.e. 3.0 and 7.0 T, which raises questions about the feasibility and practicality of these nanoparticles in modern clinical settings. With the increase of magnetic field strength in MRI scanners for clinical and preclinical applications, the effect of field strength on magnetic properties of the contrast agents has to be investigated.

Another important consideration is the exposure of nanoparticles to a biological environment, which can generate nanoparticle aggregates, which is an important yet overlooked aspect of the biological behaviour of nanoparticles [18]. Aggregation can occur when the van der Waals attractive forces between particles are greater than the electrostatic repulsive forces produced by the nanostructure surface [19, 20]. For example, a high concentration of ions can decrease the screening length of charged chemical groups on the nanoparticle surface [20] and a high concentration of protein can cause a thermodynamically favored replacement of surface-associated molecules with proteins [21], which destabilizes the nanoparticles and results in aggregation. Therefore, in biological media such as blood, saliva, lung surfactant, or cell culture media where the ion and protein contents are high, nanoparticles that are well-dispersed in a buffered solution can agglomerate. The aggregation of nanoparticles can affect cellular uptake, cytotoxicity and targeting efficiency of nanoparticles to cells and tissues [22–24]. Here we report the dependence of relaxivities on magnetic field strengths and colloid stability of 3.7 nm ultrasmall dual MRI contrast iron oxide nanoparticles.

Materials and methods

All reagents and solvents were obtained from standard commercial sources and were used as received.

Synthesis of dual contrast iron oxide nanoparticles (DCIONs)

The synthesis of the DCIONs has been described previously [5]. Briefly, thiol-functionalized poly(methacrylic acid) (PMAA-PTMP) was prepared as described elsewhere [25]. PMAA-PTMP (0.1747 g) was dissolved in miliQ-water (50 ml), purged with nitrogen to remove oxygen, and then heated to reflux. $FeCl_3{\cdot}6H_2O$ (0.1378 g) and $FeSO_4{\cdot}7H_2O$ (0.0701 g) were dissolved in concentrated HCl (1 ml). The mixture of iron precursors was quickly injected into the hot polymer solution, followed by the addition of concentrated ammonia solution (15 ml, 28%). The resultant solution was refluxed for 2 h before cooled down. The solution was concentrated and then dialyzed against miliQ-water for 72 h to remove impurities.

Aggregate synthesis

For preparation of aggregates, 20 μl of a 10× solution of NaCl was added directly to 180 μl of a pre-mixed solution of iron oxide nanoparticles (250 $\mu g\,ml^{-1}$) and bovine serum albumin (BSA, 25 $\mu g\,ml^{-1}$) under vigorous vortex mixing. To make aggregates of different sizes, NaCl were added to the final concentrations of 0, 25, 50, 100 and 200 mM.

Characterization of DCIONs and DCION aggregates

Hydrodynamic size and zeta potential of nanoparticles were determined with a Zetasizer nano series (Malvern) equipped with a 4.0 mW He–Ne laser operating at 633 nm and a detection angle of 173°. At least three measurements at 25 °C were made for each sample with an equilibrium time of 2 min before starting measurement. Transmission electron microscope (TEM) images were collected on a Hitachi HT7700 TEM operating at an accelerating voltage of 120 kV. The average size of the particles was estimated using ImageJ. X-ray diffraction (XRD) patterns were measured using a Bruker Advanced D8 Diffractometer equipped with a LynxEye detector, Cu tube and operated at 40 kV and 40 mA. Conditions of analysis are as follow: 15 rpm rotation, 2θ of 10–90° (start and end angles), 0.01° increment, 4.8 s/step time per step, 0.26° fixed divergence slit, 5.0 mm fixed anti-scatter slit. Traces were processed using the Diffrac$^{(plus)}$ Evaluation Package Release V4.2 and PDF-2 Release 2016. UV–vis absorbance spectra were obtained via a Shimadzu UV-2600 Spectrophotometer.

MRI relaxation time measurements

Measurements at 4.7 T were performed as previously described [5]. Measurements at 7 T were carried out on a preclinical MRI system, comprising a 300 mm bore 7 Tesla ClinScan, running Siemens VB17. A 40 mm ID RF coil was used to acquire the images. Measurements at 9.4 T and at 16.4 T were carried out on a 9.4 Tesla

Bruker scanner and on a 16.4 Tesla Bruker scanner, respectively. A 23 mm ID mouse head MRI RF coil was used to acquire the images. T_1 *quantification:* Spin echo images were acquired with variable TR times to calculate the T_1 time. The following parameters were used: repetition time (TR) = 100, 200, 500, 1000, 2000, 5000 ms; echo time (TE) = 8 ms (7 T), 14 ms (9.4 T), 10.5 ms (16.4 T). T_2 *quantification:* A multi TE spin echo sequence was acquired to calculate the T_2 time. The following parameters were used: TR = 2000 ms, TE = 20–400 ms in 20 ms increments.

NMR T_1 and T_2 measurements

T_1 and T_2 relaxation time measurements were performed at 298 K using Inversion Recovery and Carr–Purcell–Meiboom–Gill (CPMG) pulse sequences, respectively, on a Bruker Ascend 400 NMR spectrometer. Water solutions of iron oxide nanoparticles or aggregates were placed in Wilmad coaxial insert tubes with reference capacity of 40 μl and the tube were inserted into NMR tubes containing D_2O. Data were analyzed with TopSpin to obtain T_1 and T_2 relaxation times.

Calculation of relaxivities

Relaxivities (r_1 and r_2) are generally defined as the slope of the linear regression generated from a plot of the measured relaxation rate ($1/T_i$, where $i = 1, 2$) versus the concentration of the contrast agent (iron, Fe):

$$\frac{1}{T_i} = \frac{1}{T_{i(\text{blank})}} + r_i \cdot [Fe]$$

$$\text{or } R_i = \frac{1}{T_{i(\text{blank})}} + r_i \cdot [\text{Fe}]$$

$$\frac{1}{T_i} - \frac{1}{T_{i(\text{blank})}} = r_i \cdot [\text{Fe}]$$

T_i denotes the longitudinal and transverse relaxation times, T_1 and T_2, respectively, R_i is relaxation rate, and $T_{i(\text{blank})}$ is the relaxation times of the solvent without DCION.

Results and discussion

Synthesis and characterization of the nanoparticles

Magnetic iron oxide nanoparticles are conventionally prepared by aqueous or non-aqueous routes and the majority of preparations act as negative contrast agents [5, 26–29]. These synthetic routes mostly result in formation of large nanoparticles (diameter > 5 nm) with a large r_2/r_1 ratio. Generally, superparamagnetic iron oxide nanoparticles can shorten both T_1 and T_2 (or T_2^*) relaxation times, however, signal dephasing from reduced T_2 or T_2^* is more significant than signal enhancement due to the shorter T_1. It is because the magnetic susceptibility effect is generally dominant over longitudinal relaxation to give a much greater r_2/r_1 ratio (r_1 and r_2 are longitudinal and transverse relaxivities, respectively) than paramagnetic molecules such as Gd-DTPA [30]. Ultra-small iron oxide nanoparticles (<6 nm), on the other hand, are able to generate positive (T_1-enhanced) images due to their low magnetization resulting from a strong surface spin-canting effect [1, 5, 15, 12] and the so-called collective magnetic excitations [31]. Most ultra-small iron oxide nanoparticles have been obtained using non-aqueous synthetic routes [11–16]. The exception is particles generated by Li *et al* [5] using an aqueous route. In this study, we employed the nanoparticles synthesized by method adopted from Li *et al* [5] to study the effect of magnetic field strengths on relaxivities of these particle solutions. These nanoparticles (DCIONs) have a size of 3.7 ± 0.8 nm as shown in the TEM image (figure 1(A)). They show excellent water solubility and their hydrodynamic size was measured as 7.5 nm using dynamic light scattering (DLS). DLS provides the diameter of a sphere that moves (diffuses) the same way as the particle, assuming a hydration layer surrounding the particle. Therefore, DLS hydrodynamic size of the nanoparticle was larger than TEM size. The crystalline nature of the synthesized DCIONs was determined by XRD (figure 1(B)). The XRD peaks are characteristic of cubic structure of maghemite and magnetite. Using XRD spectrum data and the below Scherrer equation [32], the crystallite size of the nanoparticles was calculated as 4.1 nm [32].

$$L = \frac{K\lambda}{\beta \cos\theta}$$

where: L is the crystallite size of the nanoparticles; K is the dimensionless shape factor, which is typically 0.9 for sphere; λ is the x-ray wavelength; β is the line broadening at half the maximum intensity (FWHM), after subtracting the instrumental line broadening, in radians; θ is the Bragg angle. The peak at 2θ of 35.53° was chosen for the size calculation. λ was 1.54 Å and β was calculated as 0.0352 radians.

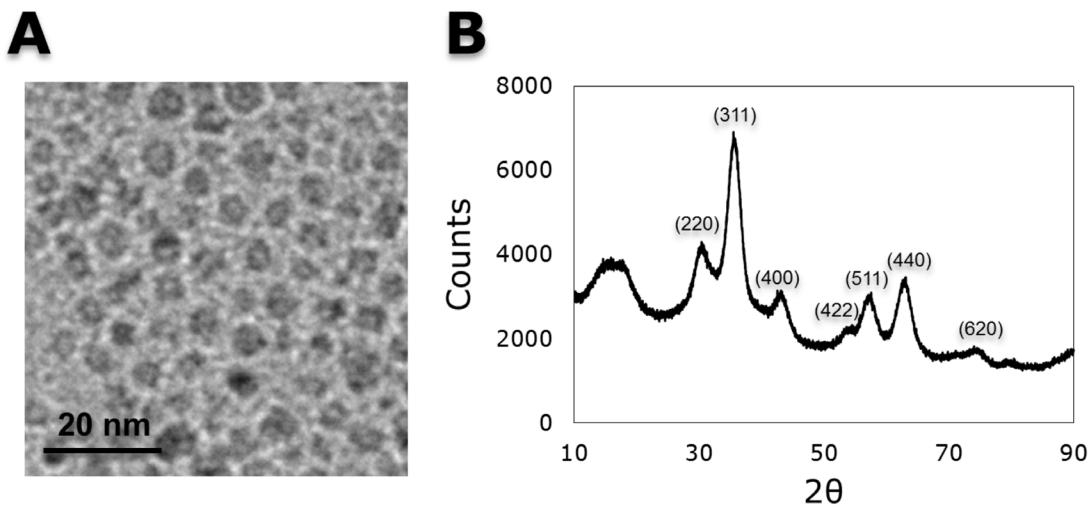

Figure 1. TEM image (A) and XRD pattern (B) of the ultra-small dual contrast iron oxide nanoparticles (DCION).

Field strength dependency of relaxivities (r_1 and r_2), and r_2/r_1 ratio

The efficiency of a MRI contrast agent is determined by its capability in lowering the longitudinal (T_1) and transverse (T_2) relaxation times of the water proton spins in tissues at the lowest contrast agent concentration [33]. The acceleration of proton relaxation near a magnetic particle is due to fluctuations of magnetic dipolar interactions between the proton spins and the electronic spins of the contrast agents. The relaxivity defined as the slope of the relaxation rate in s^{-1} (either $1/T_1$ or $1/T_2$) versus the equivalent ion concentration in mM is a direct measurement of this efficiency [33].

In this study, relaxation rates ($R_i = 1/T_i$, where $i = 1$ or 2) of DCION solutions were measured at 4.7, 7, 9.4 and 16.4 T and plotted against the Fe concentration in figure 2. From these plots, relaxivities of DCION solutions were obtained and then plotted against magnetic field strengths in figure 3. It was found that r_1 significantly decreased as the magnetic field strength increased (figure 3(A)). On the other hand, r_2 increased as the field strength increased from 1.5 T to 9.4 T and then significantly decreased at 16.4 T (figure 3(B)). Interestingly, the r_2/r_1 ratios increased with increasing the field strength (figure 3(C)), indicating the T_2 effect is the dominant effect at the high field. Since r_2/r_1 becomes very high at high magnetic field strength, any hyper-signal is lost because of spin-spin relaxation in the transverse plane where the detection antennas are sensitive [33]. Therefore, DCION may not be an effective probe for T_1-weighted positive imaging at very high magnetic field strength. Lower r_2/r_1 ratios can be favorable for T_1-weighted MRI in addition to high r_1 relaxivities. Similarly, larger r_2/r_1 ratios can be advantageous for T_2-weighted MRI in addition to high r_2 relaxivities. Similar observations were reported with gadolinium-based T_1 contrast agent [34]. Caravan *et al* found that relaxivity is clearly field dependent, susceptibility effects of Gd^{3+} are higher at higher magnetic fields, and a higher field strength leads to a lower r_1 and a higher r_2 value [34]. The consequence of these susceptibility effects is that increasing the contrast agent dose to shorten T_1 may not be effective because T_2 effects may dominate.

Dependence of relaxivities on the colloid stability of the nanoparticles

To study the dependence of relaxivities on the colloid stability of the nanoparticles, aggregation of the particles was induced. There are a number of approaches to assemble nanoparticles into controlled aggregates, including aliphatic α,ω-dithiols [35,36], light-induced self-assembly [37], DNA-directed assembly [38–42] and DNA cross-linking [43]. Here we used salt and protein which are present in the biological environment to 'naturally' induce aggregation of the nanoparticles, a process that is known to happen under 'real' conditions. By manipulating the kinetics and stoichiometry of salt (NaCl), protein (BSA) and modified-poly(methacrylic acid)-coated iron oxide nanoparticles, different levels of nanoparticle aggregation were achieved. In aqueous solution, NaCl dissociates into Na^+ and Cl^-, then Na^+ binds to the carboxylic acid groups on iron oxide nanoparticle surface, neutralizes the surface charge and induces the aggregation of nanoparticles. NaCl has been employed in aggregate synthesis for both gold and other types of nanoparticles [18, 44, 45]. BSA was used as a model protein to mimic biological media and to control the size of the aggregates. BSA stabilizes early aggregates by adsorbing proteins onto the nanoparticle surface, allowing nanoparticle assembly to defined aggregate sizes. By simultaneous addition of BSA and NaCl in various proportions (different concentrations of NaCl) to iron oxide nanoparticle solution, aggregates of different sizes were obtained (figure 4). The occurrence of aggregation was evidenced by the change in hydrodynamic size as measured with DLS (figure 4(A)); the slight change in the UV–vis absorbance spectrum (figure 4(C)); and also evidenced by TEM images (figure 4(B)). These differently-sized aggregates mimic the

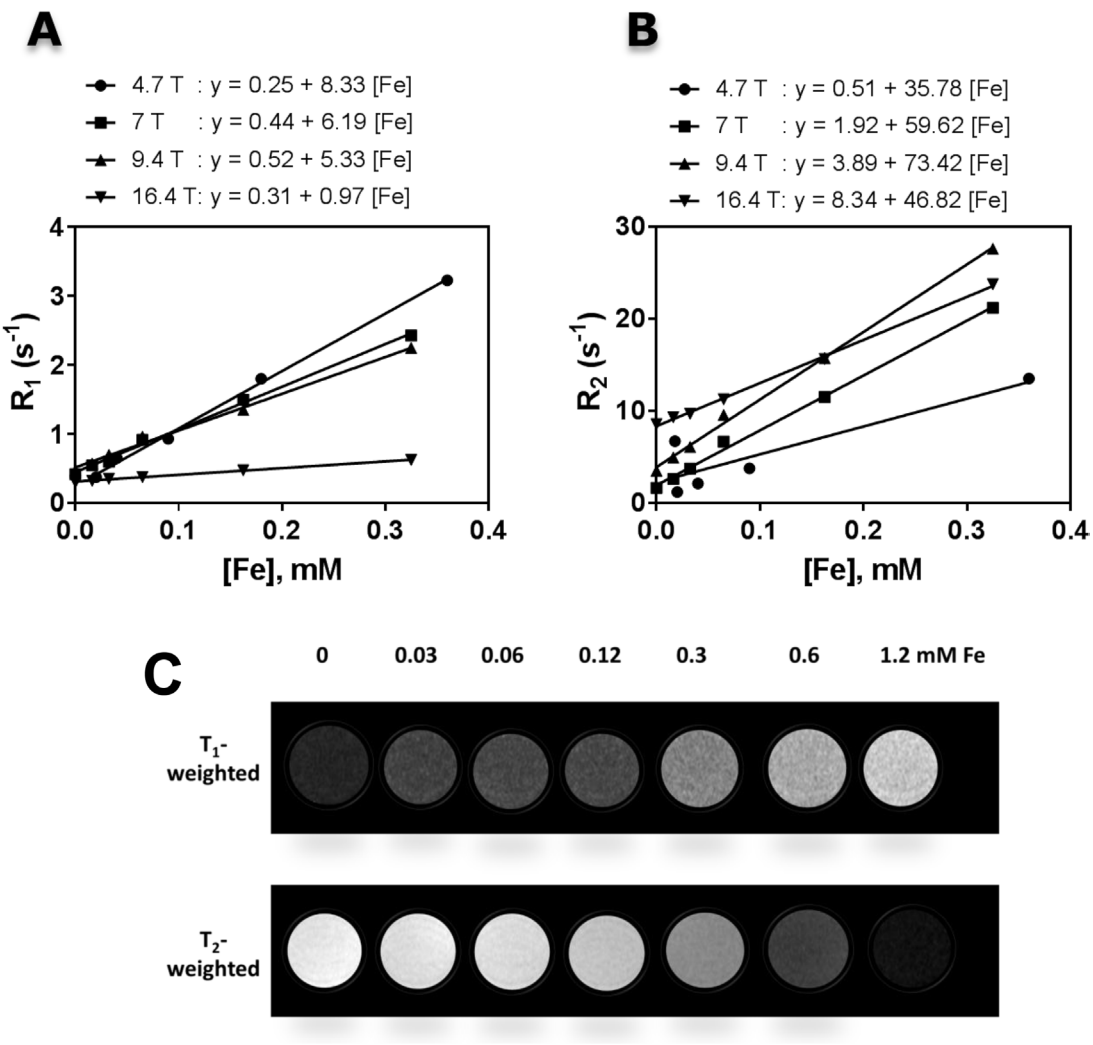

Figure 2. Plots showing longitudinal (A) and transverse (B) relaxation rates versus Fe concentrations of DCIONs at different magnetic field strengths. (C) MR images of the nanoparticle phantoms at different Fe concentration at 16.4 T field strength.

early and late stages of aggregation naturally occurring in biological environments. Initially, doublets and triplets of nanoparticles form, then aggregates progressively grow into larger structures.

Relaxivities r_1 and r_2 of aggregates were measured on a Bruker Ascend 400 NMR Spectrometer. The number-mean sizes were used to label the aggregate samples. Relaxation rates ($R_i = 1/T_i$, where $i = 1$ or 2) of the aggregate solutions were measured and plotted against the Fe concentration in figure 5. From these plots, relaxivities of aggregate solutions were obtained and then plotted against aggregate size in figure 6. It was found that as the level of aggregation or the size of the aggregates increased, r_1 significantly dropped while r_2 dramatically increased (figures 6(A) and (B)). The r_2/r_1 ratios increased with increasing size of aggregates (figure 6(C)), indicating the T_2 effect becomes dominant once these ultra-small iron oxide nanoparticles agglomerate. Iron oxide nanoparticles are able to generate large local field inhomogeneities [46]. This inhomogeneity results in a local field gradient that accelerates the dephasing of the proton spins of the water and leads to a strong reduction in the T_2 relaxation time causing a hypo-intense contrast in T_2-weighted MRI sequences. Agglomeration of multiple iron oxide nanoparticles causes higher inhomogeneity and therefore greater r_2 relaxivity. The effect of increasing r_2 relaxivity by aggregation of iron oxide nanoparticles has been described previously [47, 48]. Since T_2 effects of aggregates start to dominate the signal behavior, T_1 effects decrease, resulting in the drop in longitudinal relaxivity r_1 when nanoparticles agglomerate.

These results show that particle aggregation strongly affects relaxivities and the larger the aggregate the stronger the change in relaxivities. Methods need to be tested to stabilize the nanoparticles so they do not aggregate. Functionalization of the nanoparticles with binding ligands such as antibody for targeted molecular imaging seems to be an approach to stabilize the particles and prevent their aggregation. In our previous study, DCIONs were labelled with single-chain antibody that targets activated GPIIb/IIIa receptors on activated platelets for molecular imaging of thrombosis [3]. These nanoparticles were found to be stable in phosphate buffered saline (PBS, a buffer with 137 mM NaCl) for weeks within our study and their relaxivities remained.

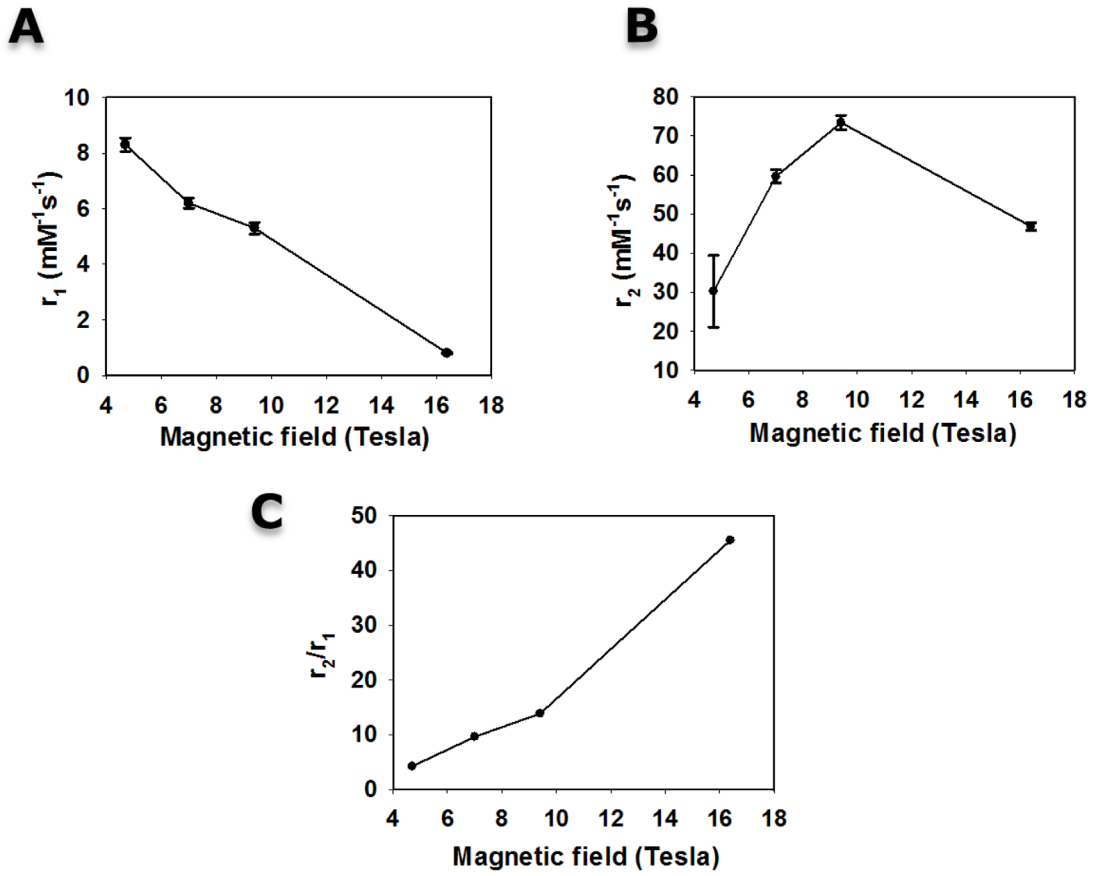

Figure 3. Dependence of longitudinal relaxivity r_1 (A), transverse relaxivity r_2 (B) and r_2/r_1 ratio (C) on magnetic field strength.

A

[NaCl], mM	Number mean	Z-Average	PDI
0	7.0 ± 0.1	15.2 ± 0.6	0.263 ± 0.031
25	11.3 ± 0.3	21.9 ± 1.2	0.324 ± 0.022
50	16.5 ± 0.3	40.7 ± 0.5	0.213 ± 0.046
100	22.8 ± 5.2	74.9 ± 0.4	0.202 ± 0.009
200	45.5 ± 4.3	117.7 ± 3.1	0.233 ± 0.009

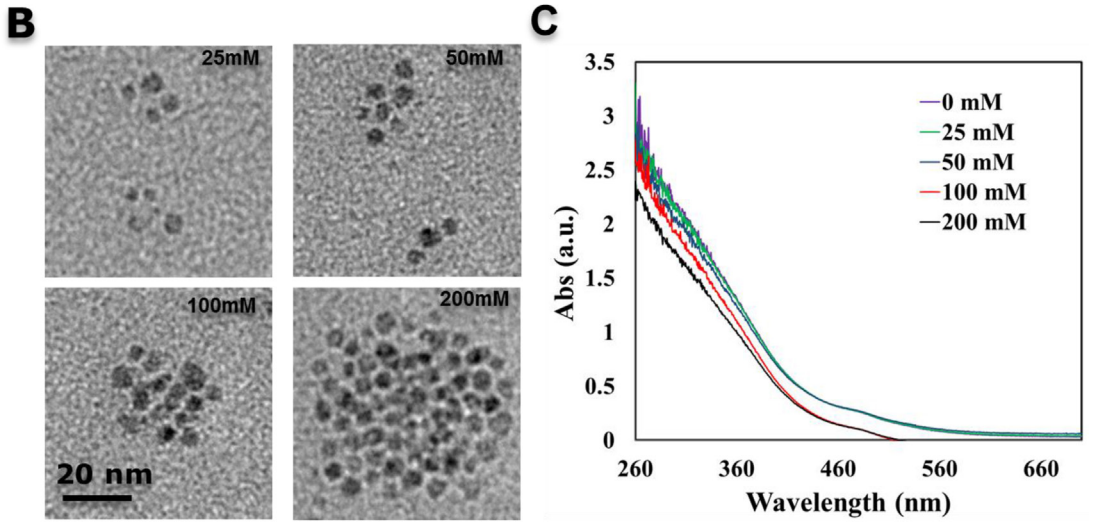

Figure 4. Characterization of the aggregates prepared using different concentrations of NaCl. (A) Hydrodynamic size and polydispersity index of aggregates, obtained by DLS. (B) TEM images of aggregates prepared using different concentrations of NaCl. (C) UV–vis spectra of aggregates.

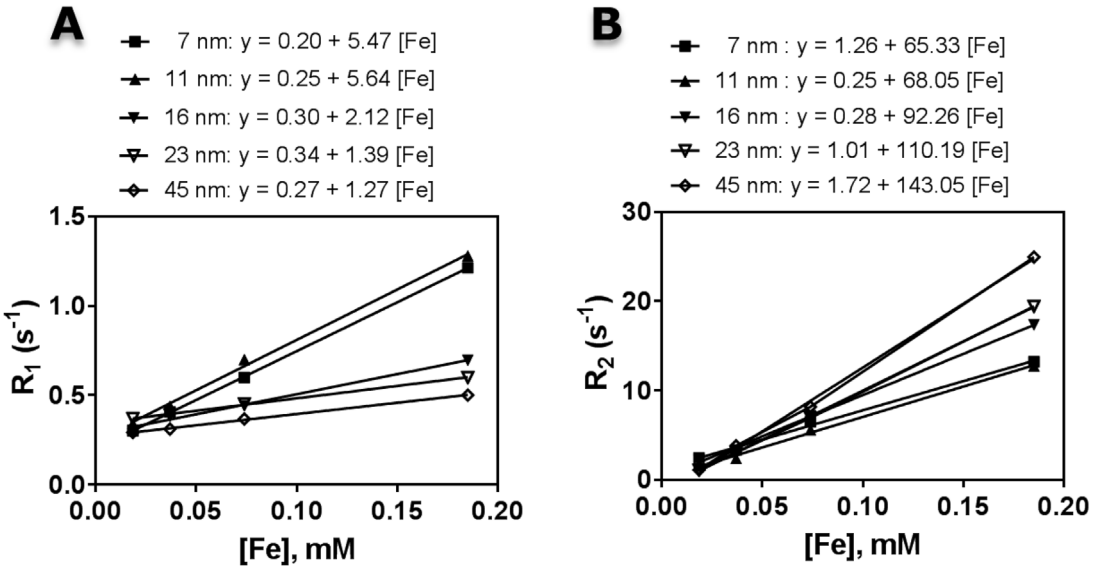

Figure 5. Plots showing longitudinal (A) and transverse (B) relaxation rates versus Fe concentrations of different-sized DCION aggregates prepared using different concentrations of NaCl. T_1 and T_2 relaxation time measurements were performed on a Bruker Ascend 400 NMR spectrometer.

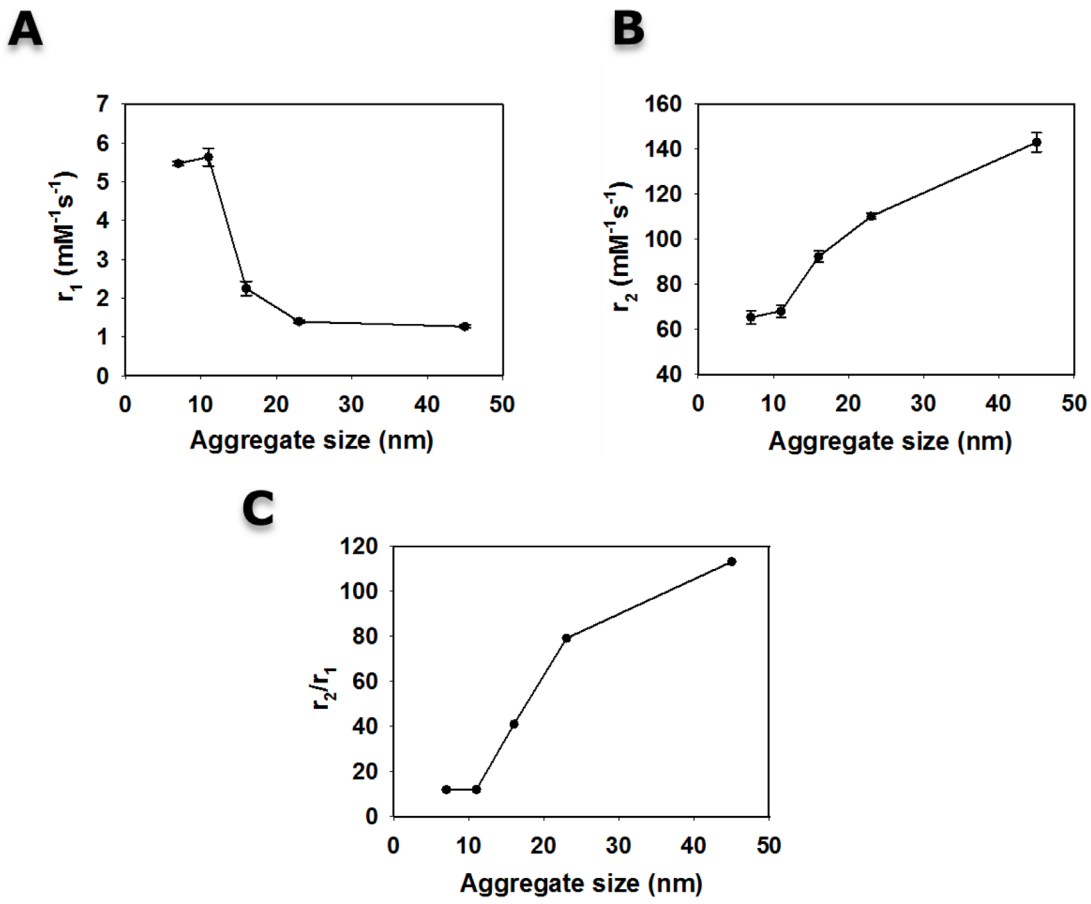

Figure 6. Dependence of longitudinal relaxivity r_1 (A), transverse relaxivity r_2 (B) and r_2/r_1 ratio (C) on the degree of aggregation or hydrodynamic size of aggregates.

Steric stabilization or functionalization of the nanoparticle surface with a hydrophilic non-ionic surfactant or neutral polymers can be a strategy to improve colloid stability of the nanoparticles in blood and physiological fluids as reviewed by Moore *et al* [49]. Poly(ethylene glycol) (PEG), a neutral polymer, is a well investigated and frequently used polymer in the field since it has been shown to avoid ionic interaction with salts present in the physiological fluids and also decrease protein adsorption. Protein-nanoparticle interaction is known to destabilize the colloidal nanoparticle system.

Conclusion

In conclusion, the presented data demonstrate the dependency of relaxivities of ultra-small positive and negative iron oxide contrast agent on the magnetic field strength and the colloidal stability. As the magnetic field strength increases from 4.7 T to 16.4 T, the longitudinal relaxivity r_1 significantly decreases while transverse relaxivity r_2 increases to its maximum at 9.4 T and then dramatically drops when the field strength increases to 16.4 T. The ratio of r_2 to r_1 also significantly increases as the field strength increases, indicating the dominance of T_2 effects. According to these findings, it is recommended that MRI employing ultra-small DCION should be avoided at very high magnetic field strengths to avoid the loss of T_1 effects, disabling their dual contrast enhancement capacity. This work investigates the dependency of relaxivity on particle aggregation induced by salt and protein, which mimics conditions in biological environments. Our results show that particle aggregation strongly affects relaxivities and the level of aggregation correlates with the extent of change in relaxivity. As the aggregate size increases, r_1 decreases while r_2 and r_2/r_1 increase, demonstrating the dominance of T_2 effects once the particles agglomerate. These findings are extremely important since aggregation appears to be an inevitable occurrence *in vivo* and will consequently affect the medical applications of dual contrast iron oxide nanoparticles. This study highlights the need for more thorough studies regarding the downstream effects of these types of contrast agents and the design of effective and stable contrast nanomaterials that are not prone to aggregate *in vivo*.

Acknowledgments

This work is funded by National Health and Medical Research Council (HTT: APP1037310), University of Queensland Early Career Grant (HTT: UQECR1606713), the Australian Research Council (AKW: CE140100036), and the National Natural Science Foundation of China (ZL: 81471657). The authors would like to acknowledge the Australian National Fabrication Facility (Queensland Node); National Imaging Facility, Centre for Advanced Imaging for access to key items of equipment. The authors also acknowledge the facilities, and the scientific and technical assistance of the Australian Microscopy and Microanalysis Research Facility at the Centre for Microscopy and Microanalysis, the University of Queensland.

ORCID iDs

Hang T Ta https://orcid.org/0000-0003-1188-0472

References

[1] Damadian R V, Goldsmith M and Minkoff L 1977 NMR in cancer: XVI. FONAR image of the live human body *Physiol. Chem. Phys.* **9** 97–100
[2] Weissleder R and Pittet M J 2008 Imaging in the era of molecular oncology *Nature* **452** 580–9
[3] Ta H T *et al* 2017 Molecular imaging of activated platelets via antibody-targeted ultrasmall iron oxide nanoparticles displaying unique dual MRI contrast *Biomaterials* **134** 31–42
[4] Phinikaridou A, Andia M E, Lacerda S, Lorrio S, Makowski M R and Botnar R M 2013 Molecular MRI of atherosclerosis *Molecules* **18** 14042–69
[5] Li Z *et al* 2012 Ultrasmall water-soluble and biocompatible magnetic iron oxide nanoparticles as positive and negative dual contrast agents *Adv. Funct. Mater.* **22** 2387–93
[6] Kircher M F, Mahmood U, King R S, Weissleder R and Josephson L 2003 A multimodal nanoparticle for preoperative magnetic resonance imaging and intraoperative optical brain tumor delineation *Cancer Res.* **63** 8122–5
[7] Nahrendorf M *et al* 2008 Nanoparticle PET-CT imaging of macrophages in inflammatory atherosclerosis *Circulation* **117** 379–87
[8] Cheon J and Lee J H 2008 Synergistically integrated nanoparticles as multimodal probes for nanobiotechnology *Acc. Chem. Res.* **41** 1630–40
[9] Gao J, Gu H and Xu B 2009 Multifunctional magnetic nanoparticles: design, synthesis, and biomedical applications *Acc. Chem. Res.* **42** 1097–107
[10] Hu F, Jia Q, Li Y and Gao M 2011 Facile synthesis of ultrasmall PEGylated iron oxide nanoparticles for dual-contrast T_1- and T_2-weighted magnetic resonance imaging *Nanotechnology* **22** 245604
[11] Kim B H *et al* 2011 Large-scale synthesis of uniform and extremely small-sized iron oxide nanoparticles for high-resolution T1 magnetic resonance imaging contrast agents *J. Am. Chem. Soc.* **133** 12624–31
[12] Neuwelt E A *et al* 2009 Ultrasmall superparamagnetic iron oxides (USPIOs): a future alternative magnetic resonance (MR) contrast agent for patients at risk for nephrogenic systemic fibrosis (NSF)? *Kidney Int.* **75** 465–74
[13] Pothayee N *et al* 2013 Magnetic nanoclusters with hydrophilic spacing for dual drug delivery and sensitive magnetic resonance imaging *J. Mater. Chem.* B **1** 1142–9
[14] Pothayee N *et al* 2012 Magnetic block ionomer complexes for potential dual imaging and therapeutic agents *Chem. Mater.* **24** 2056–63
[15] Tromsdorf U I, Bruns O T, Salmen S C, Beisiegel U and Weller H 2009 A highly effective, nontoxic T1 MR contrast agent based on ultrasmall PEGylated iron oxide nanoparticles *Nano Lett.* **9** 4434–40
[16] Wang Y X J 2011 Superparamagnetic iron oxide based MRI contrast agents: current status of clinical application *Quant. Imaging Med. Surg.* **1** 35–40
[17] Xue S *et al* 2015 99mTc-labeled iron oxide nanoparticles for dual-contrast (T_1/T_2) magnetic resonance and dual-modality imaging of tumor angiogenesis *J. Biomed. Nanotechnol.* **11** 1027–37

[18] Albanese A, Walkey C D, Olsen J B, Guo H, Emili A and Chan W C 2014 Secreted biomolecules alter the biological identity and cellular interactions of nanoparticles *ACS Nano* **8** 5515–26
[19] Verwey E O J 1948 *Theory of the Stability of Lyophobic Colloids: The Interaction of Sol Particles Having an Electric Double Layer* (Amsterdam: Elsevier)
[20] Derjaguin B and Landau L 1993 Theory of the stability of strongly charged lyophobic sols and of the adhesion of strongly charged particles in solutions of electrolytes *Prog. Surf Sci.* **43** 30–59
[21] Lundqvist M, Stigler J, Elia G, Lynch I, Cedervall T and Dawson K A 2008 Nanoparticle size and surface properties determine the protein corona with possible implications for biological impacts *Proc. Natl Acad. Sci. USA* **105** 14265–70
[22] Limbach L K *et al* 2005 Oxide nanoparticle uptake in human lung fibroblasts: effects of particle size, agglomeration, and diffusion at low concentrations *Environ. Sci. Technol.* **39** 9370–6
[23] Wick P *et al* 2007 The degree and kind of agglomeration affect carbon nanotube cytotoxicity *Toxicol. Lett.* **168** 121–31
[24] Murdock R C, Braydich-Stolle L, Schrand A M, Schlager J J and Hussain S M 2008 Characterization of nanomaterial dispersion in solution prior to *in vitro* exposure using dynamic light scattering technique *Toxicol. Sci.* **101** 239–53
[25] Huang X *et al* 2011 Biolabeling hematopoietic system cells using near-infrared fluorescent gold nanoclusters *J. Phys. Chem.* C **115** 16753
[26] Sun S and Zeng H 2002 Size-controlled synthesis of magnetite nanoparticles *J. Am. Chem. Soc.* **124** 8204–5
[27] Hyeon T 2003 Chemical synthesis of magnetic nanoparticles *Chem. Commun.* 927–34
[28] Lu A H, Salabas E L and Schuth F 2007 Magnetic nanoparticles: synthesis, protection, functionalization, and application *Angew. Chem., Int. Ed. Engl.* **46** 1222–44
[29] Laurent S *et al* 2008 Magnetic iron oxide nanoparticles: synthesis, stabilization, vectorization, physicochemical characterizations, and biological applications *Chem. Rev.* **108** 2064–110
[30] Bowers C R and Weitekamp D P 1986 Transformation of symmetrization order to nuclear-spin magnetization by chemical reaction and nuclear magnetic resonance *Phys. Rev. Lett.* **57** 2645–8
[31] Tarras-Wahlberg N, Kamali S, Andersson M, Johansson C and Rosén A 2014 Magnetization and Mössbauer study of partially oxidized iron cluster films deposited on HOPG *J. Magn. Magn. Mater.* **367** 40–6
[32] Patterson A 1939 The Scherrer formula for x-ray particle size determination *Phys. Rev.* **56** 978–82
[33] Vuong Q L, Berret J F, Fresnais J, Gossuin Y and Sandre O 2012 A universal scaling law to predict the efficiency of magnetic nanoparticles as MRI T(2)-contrast agents *Adv. Healthcare Mater.* **1** 502–12
[34] Caravan P, Farrar C T, Frullano L and Uppal R 2009 Influence of molecular parameters and increasing magnetic field strength on relaxivity of gadolinium- and manganese-based T1 contrast agents *Contrast Media Mol. Imaging* **4** 89–100
[35] Andres R P *et al* 1996 'Coulomb staircase' at room temperature in a self-assembled molecular nanostructure *Science* **272** 1323–5
[36] Brust M, Bethell D, Kiely C J and Schiffrin D J 1998 Self-assembled gold nanoparticle thin films with nonmetallic optical and electronic properties *Langmuir* **14** 5425–9
[37] Klajn R, Bishop K J and Grzybowski B A 2007 Light-controlled self-assembly of reversible and irreversible nanoparticle suprastructures *Proc. Natl Acad. Sci. USA* **104** 10305–9
[38] Nykypanchuk D, Maye M M, van der Lelie D and Gang O 2008 DNA-guided crystallization of colloidal nanoparticles *Nature* **451** 549–52
[39] Park S Y, Lytton-Jean A K, Lee B, Weigand S, Schatz G C and Mirkin C A 2008 DNA-programmable nanoparticle crystallization *Nature* **451** 553–6
[40] Sebba D S, Mock J J, Smith D R, Labean T H and Lazarides A A 2008 Reconfigurable core-satellite nanoassemblies as molecularly-driven plasmonic switches *Nano Lett.* **8** 1803–8
[41] Xu X, Rosi N L, Wang Y, Huo F and Mirkin C A 2006 Asymmetric functionalization of gold nanoparticles with oligonucleotides *J. Am. Chem. Soc.* **128** 9286–7
[42] Maye M M, Nykypanchuk D, Cuisinier M, van der Lelie D and Gang O 2009 Stepwise surface encoding for high-throughput assembly of nanoclusters *Nat. Mater.* **8** 388–91
[43] Lee S K, Maye M M, Zhang Y B, Gang O and van der Lelie D 2009 Controllable g5p-protein-directed aggregation of ssDNA-gold nanoparticles *Langmuir* **25** 657–60
[44] Drescher D *et al* 2011 Toxicity of amorphous silica nanoparticles on eukaryotic cell model is determined by particle agglomeration and serum protein adsorption effects *Anal. Bioanal. Chem.* **400** 1367–73
[45] Albanese A and Chan W C 2011 Effect of gold nanoparticle aggregation on cell uptake and toxicity *ACS Nano* **5** 5478–89
[46] Rumenapp C, Gleich B and Haase A 2012 Magnetic nanoparticles in magnetic resonance imaging and diagnostics *Pharm. Res.* **29** 1165–79
[47] Meier S *et al* 2015 Immuno-magnetoliposomes targeting activated platelets as a potentially human-compatible MRI contrast agent for targeting atherothrombosis *Biomaterials* **53** 137–48
[48] Naishun L *et al* 2016 Poly (dopamine) coated superparamagnetic iron oxide nanocluster for noninvasive labeling, tracking, and targeted delivery of adipose tissue-derived stem cells *Sci. Rep.* **6** 18746
[49] Moore T L *et al* 2015 Nanoparticle colloidal stability in cell culture media and impact on cellular interactions *Chem. Soc. Rev.* **44** 6287–305